 SL, vol.3, no.3, pp.221-238, 2010

Damage Detection in z-Fiber Reinforced, Co-Cured Composite Pi-Joint Using Pitch-Catch Ultrasonic Analysis and Scanning Laser Vibrometry

Hitesh Kapoor[1], James L. Blackshire[2] and Som R. Soni[3]

Abstract: Damage detection in constrained geometry structures like z-pinned, co-cured composite pi-joints is established using pitch-catch ultrasound and scanning laser vibrometry measurements. Ultrasonic pitch-catch measurements consisted of a network of PZT (Lead Zirconate Titanate) sensors placed on the specimen and sensing Lamb waves at each sensor location, where measurements were taken at symmetric top and bottom sensor locations for healthy and damaged pi-joint specimens. Results showed the presence of fatigue-induced bend damage of the joint as a reduced peak-to-peak amplitude response across the joint. Scanning laser vibrometry measurements were used to study the propagation of Lamb waves within the narrow, constrained geometry pi-joint structure, where the reflection and superposition of propagating Lamb waves was studied using time-resolved image analysis. The presence of delamination and hidden damage was visualized as changes in the propagating Lamb wave characteristics, where a reduction in propagating energy levels and dispersive wave characteristics were observed due to delamination and thinning of the composite plies.

1 Introduction

The in-situ health monitoring of aircraft structures is becoming an attractive alternative to traditional nondestructive evaluation (NDE) methods occurring during scheduled maintenance activities. According to Mal [Mal (2004)], 25% of an aircraft's life cost is due to maintenance and NDE requirements, which is not only costly, but is time consuming and often requires disassembly for inspections.

As a result, there is currently a need to establish reliable, efficient, and economical structural health monitoring (SHM) methodologies. For more than a decade, improvements in SHM sensor technologies and signal processing methods have been

[1] Aerospace and Ocean Engineering Dept., Virginia Tech, Blacksburg, VA-24060
[2] Air Force Research laboratory, AFRL/RXLP, WPAFB, Ohio-45433
[3] Dept. of System & Engineering Management, AFIT, 2950 Hubson Bay, WPAFB, Ohio-45433

made, which is allowing active structural health monitoring to become an integral part of a variety of aircraft structures, enhancing future aircraft safety and maintenance opportunities.

In recent years, the use of composite materials in aircraft structures has increased, where for example the newly developed Boeing B787 and Airbus A350-XWB aircraft are expected to contain nearly 50% composite materials [Croft (2005)]. Both active and passive SHM technologies are being considered for structural health monitoring of these composite structures, where ultrasonic sensing using guided Lamb waves has drawn considerable interest [Adams (2007); Giurgiutiu (2008); Staszewski et al (2009)]. In much of the work done to date, however, guided wave SHM has focused on large, open, plate-like structures typically found in wings and fuselage structures [Dalton et al (2001)]. Although these structures are of concern for SHM, structural joints are historically of critical importance for aircraft structural integrity assessments. An increasing need exists, therefore, for SHM technologies capable of characterizing complex geometry and localized joint structures in composite structures.

In this paper, the characterization of a delaminated z-pinned, pi-joint composite structure is studied using bonded Piezo-sensors and scanning laser vibrometry. The bonded Piezo-sensors were strategically placed on either side of the pi-joint, which included a varying thickness, multi-layer joint with a vertical riser. In addition, the joint included the use of z-pinned features for enhanced joint durability and reliability. Scanning laser vibrometry measurements were used to study the generation and propagation of Lamb waves through the structural joint. Both undamaged and damaged pi-joint specimens were studied, where comparisons between signal content were made with and without damage, and preliminary wave propagation analysis was accomplished to better understand Lamb wave interactions with the structure and damage features. The remainder of the manuscript includes a brief technical background on z-pinned composites and Lamb wave sensing concepts, followed by a description of the experimental studies, results, and conclusions.

2 Technical Background

2.1 Z-pinned, co-cured composite pi-joint and failure mechanisms

As pointed out recently by Russell [Russel (2007)], the increased use of composites in aerospace structures is largely dependent on reducing fabrication costs and building confidence in the strength and structural integrity of integrated, bonded joints. Although many composite joint concepts are being investigated for large-scale aircraft implementation, the “pi” joint concept has received considerable attention recently (Figure 1a), with desirable manufacturing and robust structural performance

being shown recently in coupon and full-scale aircraft testing programs [Zhang et al (2008)]. As depicted in the schematic diagram of Figure 1a, the pi-joint involves a skin-stiffener joint assembly, where the stiffener is co-cured to the skin. The design provides an inherent structural redundancy, with the pi-joint acting as two independent bondlines, resulting in improved robustness, damage tolerance, and performance characteristics.

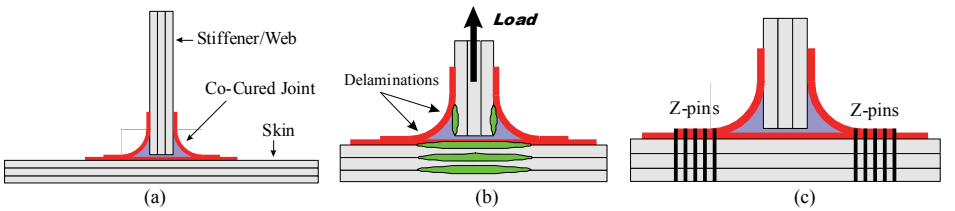

Figure 1: Composite joint concepts (a) pi-joint, (b) delamination regions, and (c) z-pinned joint reinforcement.

With regard to load-bearing strength in a composite joint structure, the energy is absorbed by matrix cracking initially, followed by the creation of fracture surfaces at the lamina interfaces, known as delamination (Figure 1b) [Kaw (2006)]. Delamination can severely impair the ability of a structure to carry load and compromises its structural integrity. Since there is a lack of natural reinforcement in the thickness direction, delamination becomes a predominant failure mode [Davidson (1994)]. In the recent past, through-the-thickness reinforcement techniques have been developed [Freitas et al (1994)], which have significantly improved the durability and reliability of composite structures [Rugg et al (2000)]. There are several 3D reinforcement technologies such as stitching, tufting, 3D weaving, and z-pinning [Freitas et al (1994); Rugg et al (2000); Dransfield et al (1994); Leong et al (2000)]. In the present research, z-pinned reinforced composite pi-joint specimens were studied (Figure 1c). A z-pin is a small diameter cylindrical rod which is embedded in a composite material and oriented perpendicular to the layer interface, enhancing the interlaminar strength of co-cured composite joint structures.

2.2 Lamb wave sensing using bonded PZT sensors

The use of guided Lamb waves in SHM applications has been studied extensively in recent years, with an increasing emphasis on the detection of damage in composite laminate materials [Monkhouse et al (1997); Wang and Chang (2000); Kessler et al (2002); Wang and Yuan (2007)]. Several excellent review articles have been written recently by Chimenti [Chimenti (2003)], Su [Su et al (2006)], and Raghavan

[Raghavan and Cesnik (2007)], in addition to books and book chapters focusing on structural health monitoring for structural composite materials [3, 4]. As pointed out by Giurgiutiu [Giurgiutiu (2005)], the appeal of guided Lamb waves for SHM applications involves its unique capability for accomplishing measurements over extended regions with a minimal number of sensors. Combined with the recent availability of inexpensive piezoelectric sensor disks, the efficient generation and use of guided Lamb waves for damage detection in thin-walled plates and shells has helped to advance SHM technologies for use many practical applications.

Guided Lamb waves involve the propagation of elastic waves in a bounded medium whose particle motion lies in the plane defined by the plate normal to the direction of wave propagation [Viktorov (1967)]. In contrast to bulk waves, guided Lamb waves involve two infinite sets of propagating modes, referred to as symmetric S_n and antisymmetric A_n modes. In most instances, the S_n and A_n modes are dispersive in nature, where the velocity of a propagating mode, c_n, depends on the ultrasonic frequency, the elastic constants and density of the material, and the ratio of the plate thickness, d, and propagating mode wavelength, λ, which determine the effective stiffness of the plate [Adams (2007); Giurgiutiu (2008); Viktorov (1967)]. For a given thickness d and frequency f, the characteristic propagating modes and wave velocities can be established using dispersion curves calculated from the Rayleigh–Lamb relations [Adams (2007); Giurgiutiu (2008); Viktorov (1967)].

It is widely known that the phenomenon of velocity dispersion can lead to significant complexity with respect to experimentally observed Lamb wave signals. As a result, the use of single mode, or 'tuned', excitation methods have been developed, where a single fundamental mode is preferentially excited and other modes are suppressed. As originally described by Giurgiutiu [Giurgiutiu (2005)], the direct shear-layer coupling between an adhesively bonded piezoelectric sensor disk and a structure can lead to an inherent and preferred coupling of energy into a particular Lamb wave mode by frequency tuning. This represents a key feature for minimizing signal complexity in a practical Lamb wave measurement process, when significant geometric and material complexity exists. The fundamental A_0 mode, for example, can effectively be isolated for generation and detection purposes, where previous research has shown an enhanced interaction of A_0 energy with delamination in composite laminates [Giurgiutiu (2005)]. The simplification of signal content from reflected energy in constrained geometric structures is also anticipated with mode isolation and frequency tuning.

2.3 Characterization of Lamb waves using scanning laser vibrometry

The propagation of elastic waves in a material can involve a number of complex physical phenomena, resulting in both subtle and dramatic effects on detected signal content. In recent years, the use of advanced methods for characterizing and imaging elastic wave propagation and scattering processes has increased, where for example the use of scanning laser vibrometry has been used very effectively to identify propagating modes, scattering phenomena, and damage feature properties [Leong et al (2005); Longo et al (2010)]. A typical scanning laser vibrometry system provides a means for measuring the local velocity or displacement levels on a material surface with spatial resolutions approaching 1 micron. In addition, because a laser beam is used to probe the material surface, the measurements are provided in a non-contact and non-interfering manner. When combined with a contact transducer for elastic wave generation, a scanning laser vibrometry system can provide time-resolved and time-averaged image results over extended areas, where wave velocity, attenuation, and scattering processes can be resolved and studied with a high degree of fidelity and spatial resolution. For constrained geometry composite materials, the use of a scanning laser vibrometry measurement provides a means for understanding Lamb wave reflection, scattering, dispersion, and mode-conversion processes, which can be used to understand signal content in a distributed bonded piezoelectric sensor array measurement used in SHM applications.

3 Test Article and Experimental Measurements

3.1 Pi-joint composite test articles

Figure 2 provides a schematic cross-sectional diagram of a pi-joint composite test article, and digital images of a sample showing bonded Piezo-sensors and composite layers in cross-section. The sample includes a 40-ply, quasi-isotropic lay-up $[0/90/45/\text{-}45]_{5S}$ for the graphite fiber/epoxy composite skin (Newport Adhesives and Composites, NCT-350-GT145-TR50S), which was co-cured with a 20-ply vertical riser/web lay-up $[0/45/90/\text{-}45/\text{-}45/45/45/90]_S$, where 1/2 of the web plies were split and re-directed 90-degrees into the top surface of the skin during the curing process. The overall length, width, and thickness of the skin region were 202.4 mm, 51 mm, and 4.8 mm, respectively. In the overlap region of the skin, the thickness increases to 6.6 mm due the additional 2 composite plies, while the thickness of the vertical riser/web region was 2.45 mm with an overall height of 140 mm. The thickened region extends out $\sim$42.8 mm on either side of the vertical riser/web region along the length of the sample, and includes 25 rows of z-pinned reinforcements (0.5 mm diameter, 4% pin density) at a nominal 1 mm spacing distance.

As shown in the upper left inset image and schematic diagram in Figure 2, eight

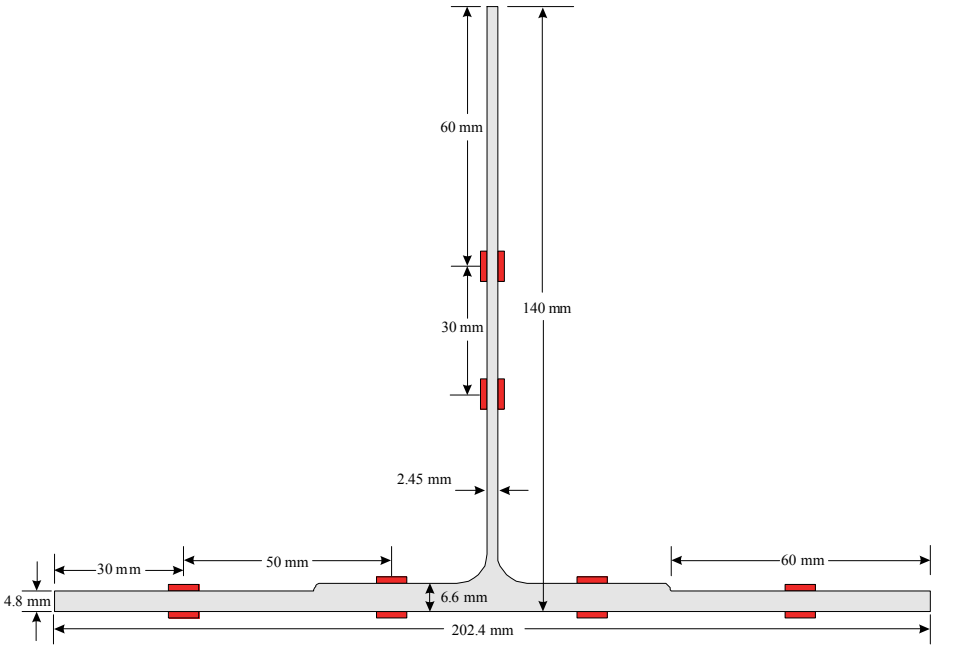

Figure 2: Schematic cross-sectional diagram of the pi-joint composite sample, and digital images of pi-joint specimen with bonded piezo sensors and cross-section details.

piezoelectric sensors (APC D-6.35mm-0.2mm-850WFB) were placed symmetrically on the top and bottom surfaces of the skin, with four additional sensors placed symmetrically on either side of the web. The sensors were bonded to the specimen using M-Bond adhesive, and were located along the length and height of the specimen as depicted in Figure 2. The sensors were 6.35 mm round disks of PZT, with a thickness of 200 microns, and polarized to produce a radial shearing force when actuated.

3.2 Experimental measurement systems

The primary equipment used in the pitch-catch ultrasound and scanning laser vibrometry experimental work is shown in Figures 3a and 3b, respectively. The pitch-catch ultrasound equipment included an Agilent 33250A arbitrary waveform generator and a LeCroy Waverunner LT584 digital oscilloscope. The function generator sent a 5-cycle, 10 Vpp, sinusoidal signal at 100 kHz to one of the bonded piezoelectric sensors, while the digital oscilloscope was used to capture the received signals at the remaining sensor positions with a 20 MHz sampling rate. An average of 100

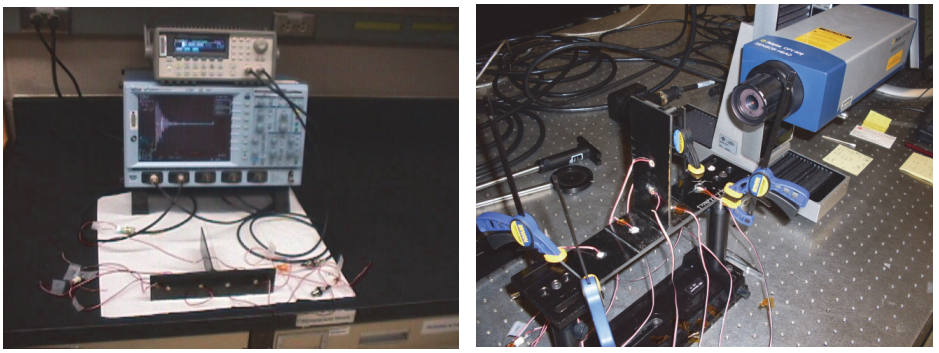

Figure 3: Data collection systems (a) pitch-catch piezo sensors, and (b) scanning laser vibrometry.

signal repetitions was made for each measurement, where a pulse repetition rate of 10 milliseconds was utilized to allow for previous signals to damp out adequately. Measurement results were obtained before and after damage had been introduced into the pi-joint material samples.

The scanning laser vibrometry system included a Polytec OFV 505 sensor head and OFV 5000 controller unit. As shown in Figure 3b, the sensor head was mounted on a 2-axis translation system, which provided 200 mm x 200 mm scan sizes at sub-micron raster-scanned step spacings. Measurements were accomplished by actuating one of the bonded piezoelectric sensors and scanning the laser interferometry beam relative to the sample surface to acquire out-of-plane displacements on the pi-joint sample surface. Sensor actuation was provided by a 10 Volt toneburst sinusoidal signal generated using the Agilent 3350A arbitrary waveform generator. The system was fully automated, utilizing custom Labview control software for data acquisition and post-processing of the captured signals with a 10 MHz sampling rate.

3.3 Fatigue testing of pi-joint composite test articles

The composite pi-joint specimens were subjected to 3-point bend tests using a 20-kip MTS load frame as depicted in Figure 4. The samples were gripped on either end of the skin and on the upper portion of the vertical riser/web as depicted in the figure, which created a bending force at the web-skin joint resulting in delamination between plies, fiber buckling, matrix cracking, and flange delamination. All tests were run at a displacement rate of 0.02 in/min. Damage in the test specimens included initial matrix cracking and delamination in the resin rich area, which grew

vertically into the web region, and secondary cracking and delamination in the lower skin region at the mid-line of the sample as depicted in Figure 4b [Freel (2006)].

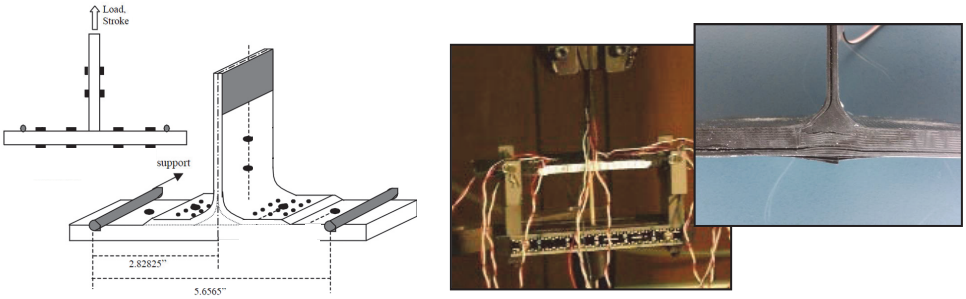

Figure 4: (a) Schematic of 3-point bend testing geometry, and (b) digital images of pi-joint specimen being load tested and resulting damage in specimen.

4 Scanning Laser Vibrometry Characterization of Lamb Wave Proagation in Constrained Geometry Pi-Joint

Scanning laser vibrometry measurements were used to study Lamb wave propagation in the constrained geometry pi-joint composite specimens. Typical results are provided in Figures 5 and 6, which depict spatially-resolved, out-of-plane surface displacement 'snapshot' images for increasing time steps from 5 to 45 microseconds in 5 microsecond steps. As shown in the images, scanning laser vibrometry measurements provided a means for visualizing ultrasonic wave propagation and scattering characteristic within the complex geometry material system. The scan dimensions in Figures 5 and 6 included a 200 mm x 50 mm scan area with 1 mm spatial steps. Bonded piezoelectric sensor actuation was accomplished using a sensor on the top left surface of the skin as indicated in Figure 5, with displacement measurements ranging from -20 and +20 nanometers, and image contrast scaled using the 8-bit gray-scale look-up-table (LUT) in Figure 5.

It is well known that the A_0 mode is less dispersive and more sensitive to composite delamination damage due to its inherent anti-symmetric motions [Giurgiutiu (2005)]. For this reason, frequency-tuned A_0 Lamb waves were preferentially excited by the bonded PZT transducer in Figures 5 and 6 using a 100 KHz, 10 volt, 5-cycle toneburst input signal. As depicted in Figures 5 and 6, the Lamb waves propagated in a circular wave energy pattern, and were quickly reflected by the

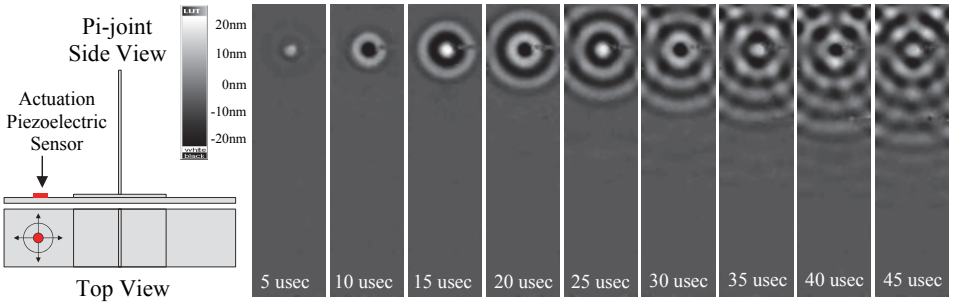

Figure 5: Time-resolved scanning laser vibrometry images of out-of-plane displacement component of A0 Lamb wave mode acquired on bottom surface of z-pinned, co-cured composite pi-joint specimen.

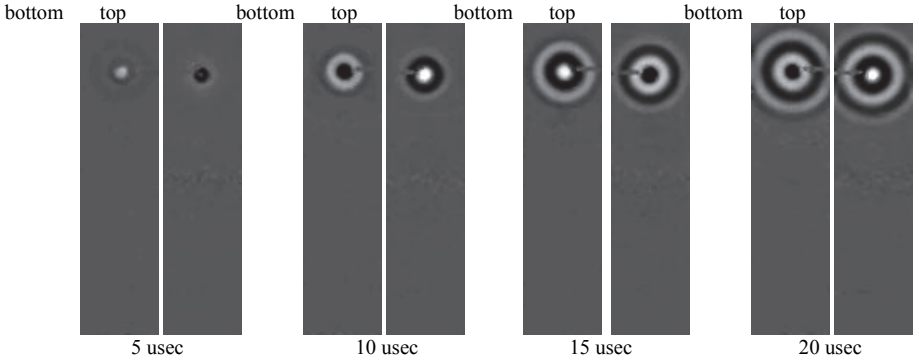

Figure 6: Scanning vibrometry displacement images showing anti-symmetric motion fields on the top/bottom surfaces of the z-pinned co-cured composite pi-joint, indicating frequency-tuned A_0 Lamb wave propagation.

constrained geometry edges of the sample within 20-25 μsec. Significant wave interference effects are noticed as the wave propagates away from the transducer due to increased interaction of waves reflecting from varying thickness regions, z-fiber scattering, and the side walls of the sample.

A verification of frequency-tuned A_0 Lamb wave excitation can be seen in Figure 6, where a set of complimentary measurements were made on the top and the bottom surfaces of the composite skin. In both measurement cases, the same bonded piezoelectric sensor was actuated on the top composite skin as indicated in Figure 5. Because the A_0 mode is characterized by an anti-symmetric motion of the opposing surfaces of a plate material, mirror images with opposite displacement

motion polarity would be expected for the A_0 mode, which in fact is confirmed in the images in Figure 6. An estimation of the A_0 wavelength (λ = 15 mm) and phase velocity (c_p = 1500 m/s) was also made based on the image measurement results in Figures 5 and 6, which are comparable with previously published values in a similar graphite fiber composite laminate material system [Grondel et al (2002)].

5 Bonded PZT Measurements of Constrained Geometry Pi-Joint

Pitch-catch measurement results for the bonded piezoelectric sensor disks on the undamaged pi-joint sample are provided in Figure 7, where sensor locations are indicated in Figure 7a. Specimen geometry dimensions and additional details were provided in Figure 2. In this set of experiments, measurements were targeted for the composite skin, where as described previously, 100 kHz toneburst signals were used to preferentially excite the A_0 mode in the pi-joint sample. Pitch-catch measurements were made for sensor pairs on the top and bottom of the composite skin, and also for propagating Lamb waves along the length of the sample.

Figure 7b depicts the thru-transmission pitch-catch signal for sensor pairs 1-2 and 3-4. Similar results were also obtained for the 5-6 and 7-8 sensor pair combinations. The 1-2 sensor signal has been offset vertically by 0.12 volts to provide a better comparison of the signal content. For both waveforms, there is a nominal 5-cycle signal that arrives almost immediately, which represents the signal transmission from the sensors on the top of the sample to the corresponding bottom sensors. The arrival time of the 3-4 sensor pair signal (3.2 usec) was slightly longer than the 1-2 sensor pair signal (2.5 usec) due to a thickness change from 6.6 mm to 4.8 mm, respectively. Due to the restricted geometry, reflected energy from the sides and left end of the sample occur relatively quickly in time causing signals to overlap at the various receiving sensor positions. The excitation source duration time for the 100 kHz, 5-cycle toneburst signal was 50 microseconds, which is apparent in both of the waveforms. The reflected signals from the left edge of the sample were expected to occur at approximately 40 microseconds for the 1-2 sensor combination, and at approximately 106 microseconds for the 3-4 sensor combination, which is in reasonable agreement with the observed signals in Figure 7b, where the 3 to 4 sensor pair shows a more distinct separation of signal content in the 0 – 200 microsecond time frame. Reflected signals from the sides of the sample occur at approximately 36 microseconds for both sensor pair combinations causing distortions and apparent lengthening of the waveforms. The signal content also decays away rapidly, which is typical of the type of the composite materials used.

Figure 7c and 7d depict propagating Lamb wave signals excited using sensor 1 and receiving sensors along the length of the sample. Figure 7c provides a compari-

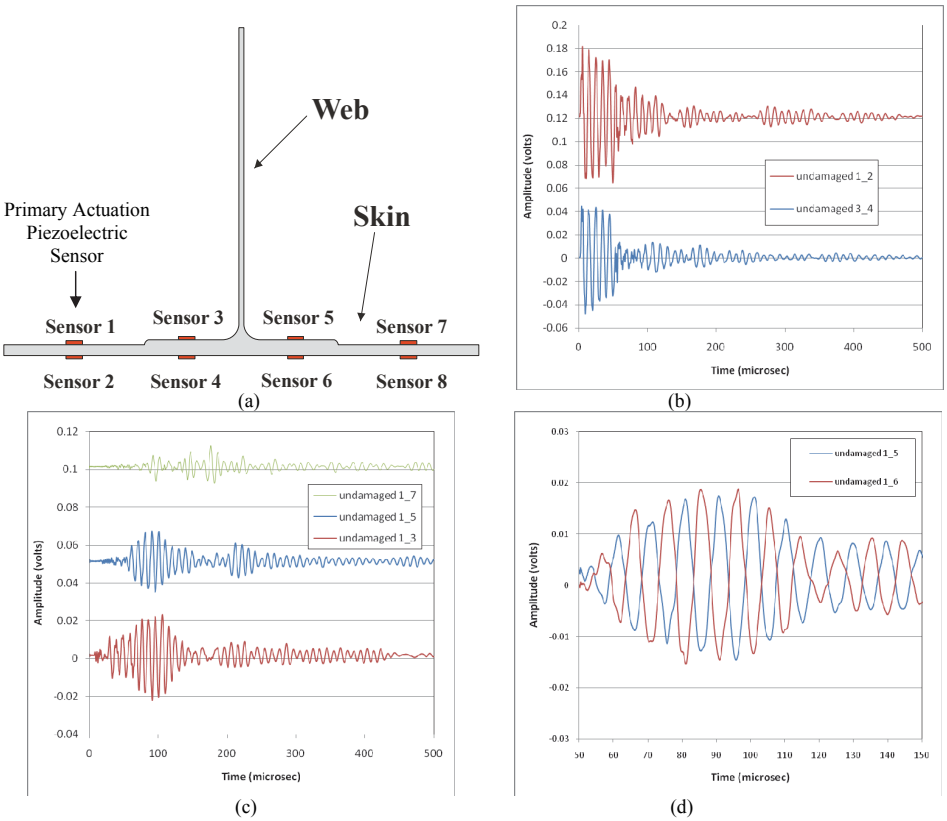

Figure 7: (a) Sensor positions locations on pi-joint sample in cross-section, (b) pitch-catch signals thru the thickness of the skin for sensor pairs 1 to 2 and 3 to 4, (c) Lamb wave signals detected along the length of the composite skin for pairs 1 to 3, 1 to 5, and 1 to 7, and (d) anti-symmetric motions detected by sensor pair from 1 to 5 and 1 to 6.

son of the signals obtained as the Lamb wave propagates at increasing distances from left to right according to the schematic diagram in Figure 7a. The 1-5 and 1-7 sensor signals have been offset vertically to provide a better comparison of the signal content. First arrival times of 33 usec, 60 usec, and 93 usec were estimated from the waveforms for the 1-3, 1-5, and 1-7 sensor pair combinations, which is in reasonable agreement with the A_0 Lamb wave mode propagating at a speed of 1500 m/s. A noticeable reduction in signal amplitudes was observed as the wave propagated due to energy spreading effects and attenuation occurring in the composite material. Reasonably consolidated toneburst signals were observed for the

1-3 and 1-5 sensor pair combinations, where the trailing toneburst signal occurring at 200 microseconds is attributed to reflected energy from the left edge of the sample. A more complex and less consolidated signal occurred for the 1-7 sensor pair combination. Similar results were observed for the 1-4, 1-6, and 1-8 pitch-catch sensor pairs. A verification of frequency-tuned A_0 Lamb wave excitation can be seen in Figure 7d, where a comparison of the 1-5 and 1-6 sensor pairs are provided showing anti-symmetric motions for the top and bottom of the sample.

6 Scanning Laser Vibrometry and Bonded PZT Sensing of Damaged Composite Pi-Joint Specimen

Figures 8 and 9 show scanning laser vibrometry results for different time snapshots of out of plane displacement for the propagating Lamb wave in undamaged (left images) and damaged (right images) z-pinned, co-cured composite pi-joint samples collected on the bottom surface and top surfaces of the composite skin, respectively. The damaged pi-joint specimen included a series of delaminated features, with the primary delamination in the skin occurring along three-quarters of the length of the sample from the right edge of the sample to the mid-point position between sensor pairs 1-2 and 3-4. This primary delamination resulted in a splitting of the composite laminate across the entire width of the sample at approximately 1.5 millimeters from the bottom of the skin. Two additional delaminated features occurred as depicted in Figure 4b, where individual plies of the composite became separated from the rest of the skin at the very bottom of the sample near the centerline along its length.

Comparing the undamaged and damaged results in Figures 8 and 9, the propagating Lamb wave patterns show dramatic changes in wavelength and amplitude characteristics, particularly at times beyond 50 microseconds. The displacement field images depicted in Figure 8 represent motion fields occurring on the bottom of the composite skin, where regions near the top of the images have not been delaminated significantly. Some shortening of the wavelength pattern can be observed in the damaged case versus undamaged case in the 30 usec images, which indicates that the delamination and material thinning has begun to occur. Because the sample thickness has been reduced, the frequency-thickness product has caused the wavelength and phase velocity to shift on the material's dispersion curve, resulting in the visual observation of a shorter wavelength pattern. As the Lamb wave continues to propagate further into the delaminated regions of the sample (50 usec, 60 usec, and 70 usec cases), a more significant wavelength-shortening effect is observed, where the delaminated thickness has been reduced to a single ply. Wave energies become very restricted in the center and lower portions of the sample due to the presence of the delamination.

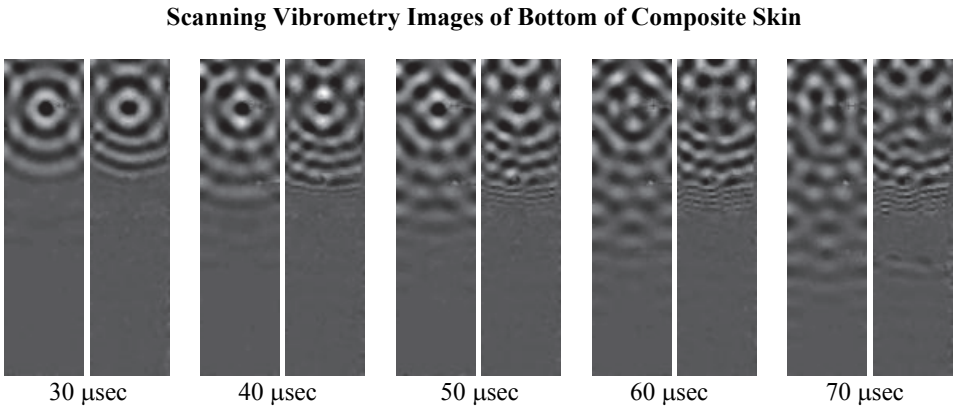

Figure 8: Scanning laser vibrometry images of out-of-plane motions for undamaged (left) and damaged (right) pi-joint composite samples for increasing times, with measurements on bottom skin surface of sample.

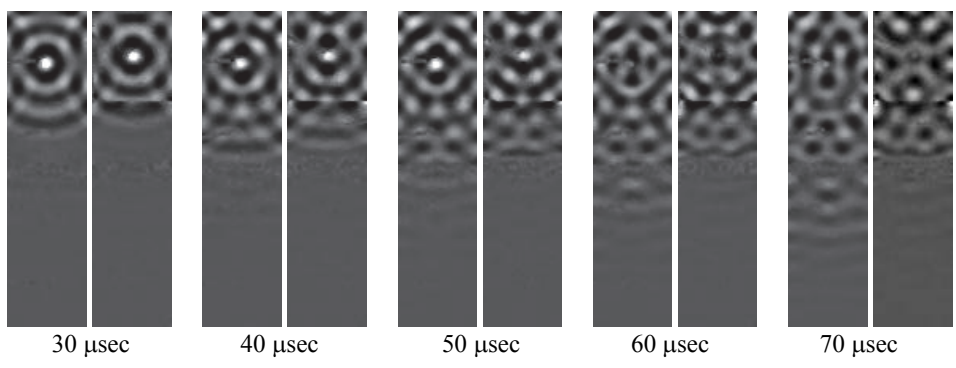

Figure 9: Scanning laser vibrometry images of out-of-plane motions for undamaged (left) and damaged (right) pi-joint composite samples for increasing times, with measurements on top skin surface of sample.

Although not as obvious, the upper surface images depicted in Figure 9 provide additional evidence of Lamb wave propagation changes for the damaged versus undamaged cases. The thickness of the upper delaminated material surface (approximately 3 mm) was relatively consistent across the length of the sample. However, as depicted in Figure 4b, additional vertically-oriented delamination features occurred in and around the resin-rich region of the composite joint, which did not

permit Lamb wave energy to propagate beyond the central portion of the material in the delaminated cases shown in Figure 9. A distinct horizontal feature also occurs in the damaged image cases near the top of the samples, which is not present in the undamaged cases. This feature is located at the position where the vertical web and skin meet and is a likely indication the joint failure mechanisms occurring in the pi-joint specimen geometry. Additional efforts are underway to better understand some of the interesting observations in these wave propagation studies with regard to failure modes in the joint.

Figure 10 provides a series of pitch-catch bonded piezoelectric measurement results for the undamaged versus damaged pi-joint cases. In all four examples, sensor 1 was used as the excitation source (see Figure 7a), where the remaining 7 sensors were used as receivers. Representative measurements are provided for the 1-2, 1-3, 1-5, and 1-7. Figure 10a provides a comparison of thru-the-thickness pitch-catch measurements for sensor pair combination 1-2. It shows nearly identical signal results for timescales below 50 microseconds, with increasing variability in signal content as time progresses. This indicates that the sample has not changed significantly near the two sensor positions, but at increasing distances reflected energy content has changed. Figure 10b provides a comparison of damaged and undamaged cases for energy propagating between sensor positions 1-3, where the delamination has begun to occur. Signal content is again similar for timescales below 50 microseconds with significant reductions in Lamb wave propagation beyond that timeframe for the damaged case. For the results depicted in Figures 10c and 10d, significant changes and reductions in signal content are evident for the damage versus undamaged cases, where the delamination have inhibited any energy propagating from left-to-right beyond the joint region and centerline of the sample in length. Some minor energy is evident, however in both cases, with increased propagation times due to the propagation of energy around the various delaminated regions, which resulted in longer travel distances. In general, evidence of damage became more pronounced as sensor separation distances increased. In addition, good agreement was observed in propagating wave features present in the scanning vibrometry versus bonded piezoelectric signals. Additional efforts are underway to correlate the two measurement results with quantitative estimates of damage features in the pi-joint samples.

7 Conclusion

The present research establishes a damage detection methodology in z-pinned, co-cured composite pi-joint samples, utilizing guided Lamb waves and bonded piezoelectric pitch-catch sensing and scanning laser vibrometry displacement field imaging. The specimen involved an advanced structural composite material joint, which

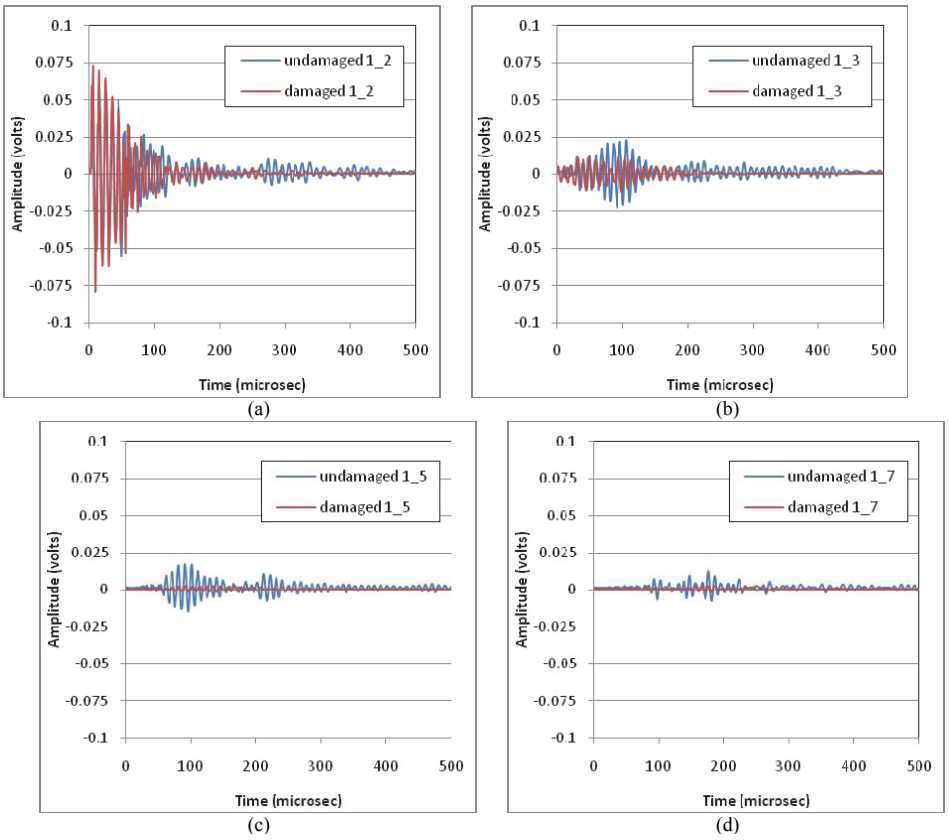

Figure 10: Pitch-catch bonded piezoelectric signals for damaged versus undamaged pi-joint cases for (a) thru-the-thickness sensor pair 1-2, (b) sensor pair combination 1-3, (c) sensor pair combination 1-5, and (d) sensor pair combination 1-7.

was complex in nature involving a constrained geometry with varying thickness and complex curvatures. The value of utilizing scanning laser vibrometry for wave propagation analysis combined with a practical distributed piezoelectric sensor network was shown, where damage sensing capabilities for structural health monitoring applications was emphasized. A direct comparison of undamaged and damaged composite pi-joint specimens was made, where complex delaminated features and restricted structural geometries were studied and discussed. Evidence of fatigue-induced bend damage of the joint was observed as reduced amplitude responses across the joint using both methods. The presence of delamination and hidden damage was visualized using the scanning laser vibrometry approach as changes in the propagating Lamb wave characteristics, where a reduction in propagating en-

ergy levels and dispersive wave characteristics were observed due to delamination and thinning of the composite plies.

References

Adams, D. (2007): Health Monitoring of Structural Materials and Components, John Wiley and Sons, New Jersey.

Chimenti, D.E. (2003): Guided Waves in Plates and their use in Materials Characterization, Appl. Mech. Rev., Vol. 50, No. 5, pp. 247-284.

Croft, J. (2005): Airbus and Boeing Spar for Middleweight Title, *Aerospace America*, pp. 36-42.

Dalton, R., Cawley, P., and Lowe M. (2001): The Potential of Guided Waves for Monitoring Large Areas of Metallic Aircraft Fuselage Structures, *J. Nondestructive Evaluation*, Vol. 20, No. 1, pp. 29-46.

Davidson, B. (1994): Prediction of Delamination Growth in Laminated Structures, In: Failure Mechanics in Advanced Polymeric Composites, AMD Vol. 196, Kardomateas, G., and Rajapakse Y., editors. American Society of Mechanical Engineers, pp. 43–65.

Dransfield, K., Baillie, C., and Mai, Y. (1994): Improving the Delamination Resistance of CFRP by Stitching – a Review, *Comp. Sci. and Tech.*, Vol. 50, No. 3, pp. 305-317.

Freel J. K. (2006): Modeling fracture in z-pinned composite co-cured laminates using smeared properties and cohesive element in Dyna-3D, Air Force Institute of Technology, MS Thesis.

Freitas, G., Magee, C., Dardzinski, P., and Fusco, T. (1994): Fiber Insertion Process for Improved Damage Tolerance in Aircraft Laminates, *J. Adv. Mater.*, Vol. 25, pp. 36-43.

Grondel, S., Paget, C., Delebarre, C., Assaad, J., and Levin, K. (2002): Design of Optimal Configuration for Generating A0 Lamb Mode in a Composite Plate Using Piezoelectric Transducers, *J. Acoust. Soc. Am.*, Vol. 112, No. 1, pp. 84-90.

Giurgiutiu V. (2005): Tuned Lamb Wave Excitation and Detection with Piezoelectric Wafer Active Sensors for Structural Health Monitoring, *Journal of Intelligent Materials Systems and Structures,* Vol. 16, No. 4, pp. 291-305.

Giurgiutiu, V. (2008): Structural Health Monitoring with Piezoelectric Wafer Active Sensors, Elsevier, New York.

Kaw, A. (2006): Mechanics of Composite Materials (2nd ed.), CRC Press.

Kessler S. S., Spearing S. M. and Soutis C. (2002): Damage detection in composite materials using Lamb wave methods, *Smart Materials and structures,* Vol. 11, pp. 269-278.

Leong, K., Ramakrishna, S., Huang, Z., and Bibo, G. (2000): The Potential of Knitting for Engineering Composites – A Review, *Composites Part A: Appl. Sci. and Manuf.*, Vol. 31, No. 3, pp. 197-220.

Leong, W., Staszewski1, W., Lee, B., and Scarpa, F. (2005): Structural health monitoring using scanning laser vibrometry: III. Lamb waves for fatigue crack detection, *Smart Mater. Struct.*, Vol. 14, No. 6.

Longo, R., Vanlanduita, S., Vanherzeelea, J., and Guillaumea, P. (2010): A method for crack sizing using Laser Doppler Vibrometer measurements of Surface Acoustic Waves, *Ultrasonics*, Vol. 50, No. 1, pp. 76-80.

Mal, A. (2004): Structural Health Monitoring, *Mechanics*, 33, pp. 6-28.

Monkhouse R. S. C., Wilcox P. W., Cawley P. (1997): Flexible interdigital PVDF transducer for the generation of Lamb Waves in structures, *Ultrasonics,* Vol. 35, pp. 489-498.

Raghavan, A., and Cesnik, C. (2007): Review of Guided-Wave Structural Health Monitoring, *The Shock and Vibration Digest*, Vol. 39, No. 2, pp. 91-114.

Rugg, K., Cox, B., and Massabo, R. (2000): Mixed Mode Delamination of Polymer Composite Laminates Reinforced Through-the-thickness by Z-fibers, *Composites Part A: Adv. Sci. and Manufact.*, Vol. 33, pp. 177–190.

Russel, J.D. (2007): Composite Affordability Initiative: Transitioning Advanced Aerospace Technologies through Cost and Risk Reduction, *AMMTIAC Quarterly*, Vol. 1, No. 3, pp. 3-6.

Staszewski, W. J., Mahzan, S. and Traynor, R. (2009): Health Monitoring of Aerospace Composite Structures – Active and Passive Approach, *Composite Science and Technology*, Vol. 69, pp. 1678–1685.

Su Z., Ye L., and Lu Y. (2006): Guided Lamb Waves for Identification of Damage in Composite Structures: A Review, *Journal of Sound and Vibration*, Vol. 295, pp. 753-780.

Viktorov, I. (1967): Rayleigh and Lamb Waves: Physical Theory and Applications, Plenum Press, New York.

Wang C. S. and Chang F. K. (2000): Diagnosis of impact damage detection of composite structures with built-in piezoelectric network, *Proceedings of SPIE,* 3990, pp. 13-19.

Wang L. and Yuan F. G. (2007): Group velocity and characteristics wave curves of Lamb Waves in Composites: Modeling and experiments, Composite Science and Technology, Vol. 67, pp. 1370-1384.

Zhang, A., Liu H., Mouritz A., and Mai, Y. (2008): Experimental Study and Computer Simulation on Degradation of Z-pin Reinforcement under Cyclic Fatigue, *Composites Part A: Adv. Sci. and Manufact*, Vol. 39, pp. 406-414.